REDOR Applications in Biology: An Overview

Orsolya Toke
Chemical Research Center of the Hungarian Academy of Sciences, Budapest, Hungary
&
Lynette Cegelski
Stanford University, Stanford, CA, USA

1 INTRODUCTION

Rotational echo double resonance (REDOR) is a solid-state NMR technique that provides a direct measure of short and long-range heteronuclear dipolar couplings, typically between pairs of rare spins.[1] The couplings contain information on both internuclear distances and orientations[2] so that REDOR can serve as a spectroscopic ruler and protractor. REDOR can also be used as a spectroscopic selection tool to filter spectra based on dipolar couplings, in order to monitor metabolic pathways or to compare particular molecular densities among samples. Since its introduction in 1989, REDOR has been employed by many labs around the world in biological chemistry as well as in polymer chemistry and materials science. In each of these fields, the REDOR strategy is generally not one of total-structure determination, but rather one of accessing site-specific atomic-level information to examine composition and to probe structure, dynamics, and metabolism in heterogeneous, noncrystalline, insoluble systems as complex as bacterial whole cells and intact plant leaves. In biology, REDOR has also found applications in the characterization of binding sites of proteins, amyloid fibers and plaques, and in the analysis of noncrystalline, poorly soluble heterogeneous molecular systems such as membrane protein helical bundles, membrane-associated antimicrobial peptides, and bacterial cell walls. The overall REDOR approach to biological systems is powerful, versatile, and broadly applicable to diverse systems; yet the experimental protocol, including the isotopic labeling strategy, sample preparation, and NMR measurement, depends on the system at hand and the questions being addressed. Thus, the REDOR approach is best appreciated and understood by way of example. In this article, we provide a short summary of REDOR NMR methodology, followed by a survey of recent applications to highlight the problem-solving versatility of REDOR in biological systems.

2 REDOR METHODOLOGY

2.1 REDOR Access to Dipolar Couplings

The dipole–dipole coupling between heteronuclei within a magnetic field, i.e., the interaction between the magnetic moments of the nuclear spins, is described by the truncated dipolar Hamiltonian as in equation (1).

$$\mathcal{H}_{\mathrm{D}} = \omega_{\mathrm{D}} I_{\mathrm{Z}} S_{\mathrm{Z}},\ \omega_{\mathrm{D}} = \frac{3\cos^2\theta - 1}{2} \cdot D,\ D = \frac{\gamma_1 \gamma_2 \hbar}{\boldsymbol{r}^3} \qquad (1)$$

The dipolar Hamiltonian depends on both spatial and spin coordinates. The dipolar coupling (D) contains the crucial distance and orientation information. The angle, θ, is the angle between the $I-S$ internuclear vector and the applied magnetic field; γ_1 and γ_2 are the gyromagnetic ratios of the I and S nuclei; $\hbar$ is the reduced Planck constant; and $\boldsymbol{r}$ is the internuclear vector between the two spins. Notably, the dipolar coupling strength, D, is proportional to the inverse third power of the internuclear distance and thus is extremely sensitive to the separation of the coupled spins.

Magic-angle spinning (MAS) averages over the spatial coordinates and suppresses the dipolar interaction, but in a coherent manner. The REDOR measurement uses the application of rotor-synchronized radiofrequency pulses to operate exclusively on the spin coordinates, imposing another coherent process of comparable frequency, to interfere with the complete suppression of the dipolar coupling by MAS.[1] The extent to which the manipulation of the spin coordinates defeats the averaging that results from MAS is a measure of the dipolar coupling which yields internuclear distances. Orientation information is preserved in the sidebands of the high-resolution spectrum acquired under MAS, and analytical expressions have been described for these.[2] The recoupling, or reintroduction of the dipolar coupling, is also the basic principle for the myriad of homonuclear recoupling techniques that are used to measure dipolar couplings.[3,4]

2.2 The REDOR Measurement

REDOR is performed in two parts (Figure 1a), once with rotor-synchronized dephasing pulses (S) and once without (full echo, S_0). Maximum intensity rotational echoes are formed at the end of each rotor period when no dephasing pulses are applied. During the second half of the measurement, rotor-synchronized π pulses are applied to the dephasing spin. One π pulse applied in the center of the rotor period changes the sign of the heteronuclear dipolar coupling and defeats the averaging of the dipolar coupling by MAS. The second pulse, coincident with the rotor period serves to add the dephasing of subsequent rotor periods. The difference in signal intensity ($\Delta S = S_0 - S$) for the observed spin in the two parts of the REDOR experiment is directly related to the corresponding distance to the dephasing spin.

eMagRes, Online © 2007 John Wiley & Sons, Ltd.

This article was previously published in the *Encyclopedia of Magnetic Resonance* in 2010 by John Wiley & Sons, Ltd.
DOI: 10.1002/9780470034590.emrstm1152

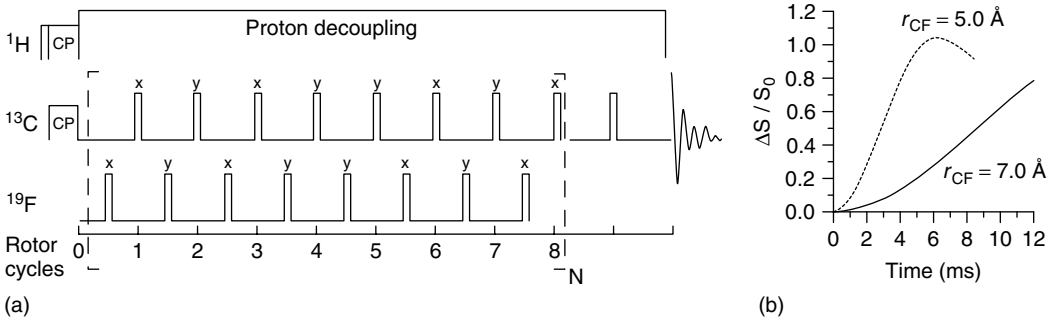

Figure 1 The REDOR measurement. (a) REDOR is performed in two parts, once with dephasing pulses (S spectrum) and once without (full echo, S_0 spectrum). REDOR spectra are typically collected with standard xy-8 phase cycling,[5] on both observed and dephasing channels. (b) The difference in signal intensity for the observed spin in the two parts of the REDOR experiment is directly related to the corresponding distance to the dephasing spin and is plotted as $\Delta S/S_0$ as a function of evolution time

More specifically, the application of π pulses flips the spins. This changes the sign of the dipolar coupling for observe spins coupled to the dephasing spin, leading to a reversal in the sense of rotation of the observe spins. When no dephasing pulses are applied, the average dipolar coupling between two nuclei over one rotor period is zero. The application of dephasing pulses reveals the coupling and produces an average precessional frequency, $\omega D\ (\alpha,\ \beta,\ t)$ for each coupled spin in the powder.[1] Thus, phase accumulates and leads to signal loss. The encoding of phase through dipolar transitions is more obvious by inspection of the expression for ωD in equation (2)

$$\overline{\omega_D} = \pm\frac{D}{4\pi}\left\{\sin^2\beta[\sin 2(\alpha+\omega_r t_1) - \sin\ 2\alpha] - (2\sqrt{2}\sin 2\beta[\sin(\alpha+\omega_r t_1) - \sin\alpha]\right\} \quad (2)$$

where D is the dipolar coupling, given earlier; α and β are the azimuthal and polar angles, respectively, in a coordinate system with the z-axis parallel to the rotor axis; ω_r is the spinning frequency; t_1 is the time of application of the π pulse from the start of the rotor period. The time for which this coupling operates in the REDOR measurement is termed the *dipolar evolution time* ($N_r \times t_r$). Each spin accumulates a net phase due to dipolar transitions during this time, as defined in equation (3)

$$\Delta\phi = \overline{\omega_D}(\alpha, \beta; t_1)t_r N_r \quad (3)$$

where $\Delta\phi$ is the accumulation of phase; t_r is the time of one rotor period; and N_r is the number of rotor cycles. Thus, the dipolar coupling is manifested as signal attenuation at the end of every rotor period. Therefore, weak couplings, i.e. spins with a small average dipolar transition frequency, can be amplified by increasing the number of rotor cycles (N_r) over which the dephasing occurs or by simply spinning slower (t_r). By measuring the observed intensity loss as a function of time ($N_r t_r$), one can deduce the heteronuclear dipolar coupling.

Calculated REDOR curves are compared with the signal intensity or, as shown in Figure 1(b), with the fraction of the signal difference and the reference intensity, as a function of the dipolar evolution time to determine the heteronuclear dipolar coupling constant and therefore the distance between the two spins.

2.3 REDOR Variations

Several modifications to the traditional REDOR measurement have been implemented and optimized for use in specific systems. RDX permits heteronuclear distance determinations in a spin system not reducible to representation by an isolated spin pair, for the case of the dipolar coupling of a single dephasing spin to a cluster of observed spins.[6,7] Frequency-selective REDOR allows the application of dephasing pulses to a chemically shifted spin of interest. This is particularly useful to determine distance and orientation dephasing parameters involving a shift-resolved carbon resonance, for example, without contributions from other carbons in the system. Dante-pulse frequency-selective irradiation that uses a series of short pulses[8,9] has been used in biological applications,[10–12] and a frequency-selective single Gaussian pulse has also been described.[13] Additional REDOR variants include TEDOR–REDOR (rotational echo double resonance–transferred echo double resonance),[14] double-REDOR,[15] and FRESH.[16] These three variants require a four-frequency radio frequency probe and empower the spectroscopist to make selective assignments and measurements even in the presence of overlapping natural abundance or labeled resonances. REDOR has also been adapted to measuring dipolar couplings between protons and heterospins, permitting the determination of longer-range distances due to the high-gyromagnetic ratio of protons.[17–19]

3 MEMBRANE PEPTIDES, PROTEINS, AND STEROLS

With the employment of site-specific ^{13}C, ^{15}N, ^{19}F labeling, dipolar recoupling experiments under MAS conditions provide an opportunity to obtain high resolution distance restraints for polypeptide chains embedded in membrane environments. These intra- and intermolecular distance restraints can be used to probe various properties of membrane peptides and proteins including conformation, aggregation, and location in the bilayer. In conjunction with other CPMAS and static solid-state NMR experiments, complete descriptions of the structure, depth of insertion, and orientation of polypeptide chains can be generated.

eMagRes, Online © 2007 John Wiley & Sons, Ltd.

This article was previously published in the *Encyclopedia of Magnetic Resonance* in 2010 by John Wiley & Sons, Ltd.
DOI: 10.1002/9780470034590.emrstm1152

3.1 Mapping Location in the Bilayer

The phosphorus atom in phospholipid head groups is a natural label that can be used in mapping peptide, protein, and guest molecule locations in bilayers. By incorporating ^{13}C or ^{15}N labels at various locations in a peptide sequence or a guest molecule, such as cholesterol or other sterols, $^{13}C\{^{31}P\}$ and $^{15}N\{^{31}P\}$ REDOR experiments can be used to determine comparative proximities to the lipid head groups. We should note that phosphate head groups in lipid bilayers create a system where there are multiple ^{31}P dephasers, whose contributions are difficult to deconvolute. Distance measurements with multiple dephasers are model dependent and, for bilayers, require knowledge of the lipid areas (to yield the spacing of the ^{31}P atoms), as well as the orientation of $^{13}C-^{31}P$ dipolar tensors. Nevertheless, comparative REDOR dephasing and relative proximities can provide crucial parameters to understand biological properties and function. In addition, fluorinated lipids, in which lipid tails are terminated in ^{19}F, can provide an NMR probe at the center of the bilayer. This type of lipid cartography was recently applied to identify the spatial preferences of three sterols in ^{19}F-labeled dipalmitoylphosphatidylcholine (DPPC) phospholipid multilamellar vesicles: 17β-estradiol (estradiol); 17β-estradiol 17-benzoate (estradiol benzoate); and 17β-2-(1-adamantyl) estradiol (adamantyl estradiol).

Several sterols, including derivatives of 17β-estradiol, are of interest for their potent antioxidant and neuroprotectant activities, and they have become the focus of drug development efforts aimed at treating and preventing neuronal damage in stroke-related brain damage, Alzheimer's disease, and Parkinson's disease. $^{13}C\{^{31}P\}$ and $^{13}C\{^{19}F\}$ REDOR were used to map the placement of a panel of related estrogen molecules in multilamellar vesicles.[20] The readily determined qualitative differences among the sterols correlated with their neuroprotective potencies. The REDOR dephasing of ^{13}C by ^{31}P in the head group and by ^{19}F at the lipid tails (sparsely fluorinated), provided a measure of sterol proximity to ^{31}P and ^{19}F with respect to lipid atomic landmarks: lipid headgroup carbons, the carbonyl carbons, and the methyl tails. In effect, dephasing of the landmarks define lines of latitude in the lipid bilayer. Thus, each set of REDOR spectra contains information about lipid–lipid and sterol-lipid contacts.

The spectra in Figure 2 illustrate the mapping strategy for two separately labeled samples of 17β-estradiol 17-benzoate (estradiol benzoate), one in which the ^{13}C atom is proximate to the head groups and one in which it is distant. At short evolution times, the $^{13}C\{^{31}P\}$ REDOR measurement serves as a short-range ruler, identifying carbons that are near phosphorus. The lipid carbonyl carbon peak at 172 ppm was dephased by 50%, which represents an average dephasing for both carbonyl carbons, after an evolution time of 8.96 ms (64 T_r) (Figure 2a). Because the label of [3-^{13}C]estradiol benzoate (Figure 2a) had a $^{13}C\{^{31}P\}$ REDOR difference comparable to that of the lipid carbonyl carbons (57%), the sterol label was mapped in the same vicinity as the lipid carbonyl-carbon landmark. The lipid head group $^{13}C\{^{31}P\}$ dephasing (60–70 ppm) was nearly 100%, expected for 2–5 Å distances. At this short evolution time, there was no contact for the lipid methyl carbons (14 ppm) and only weak contact for acyl chain aliphatics (30 ppm). The nearly undetectable REDOR dephasing in the estradiol [1-^{13}C] benzoate spectra indicated that this carbon was distant from ^{31}P (Figure 2b). Subsequent $^{13}C\{^{19}F\}$ REDOR confirmed that the estradiol [1-^{13}C]benzoate label was near to the lipid tails labeled by-CH_2F.

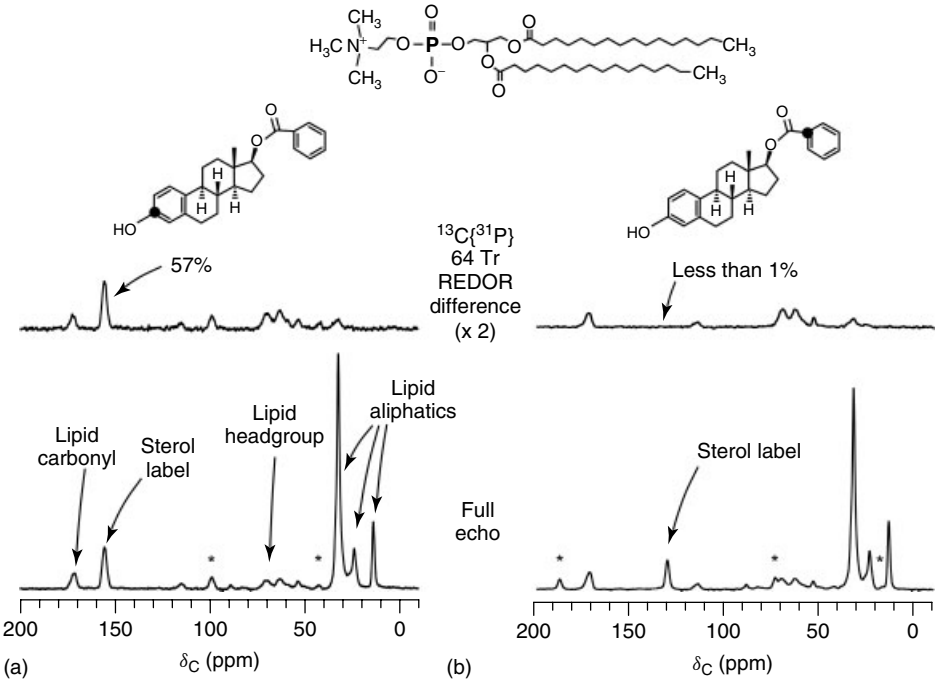

Figure 2 (a) Lipid cartography by REDOR. 125-MHz $^{13}C\{^{31}P\}$ REDOR spectra of [3-^{13}C]estradiol benzoate and (b) estradiol [1-^{13}C]benzoate in a lipid bilayer after 64 rotor cycles (8.96 ms) of dipolar evolution with MAS at 7143 Hz. The full-echo spectra are shown at the bottom of the figure and the REDOR difference spectra at the top. Spinning sidebands of peaks corresponding to the sterol labeled carbons (solid circles) are marked by asterisks

eMagRes, Online © 2007 John Wiley & Sons, Ltd.

This article was previously published in the *Encyclopedia of Magnetic Resonance* in 2010 by John Wiley & Sons, Ltd.
DOI: 10.1002/9780470034590.emrstm1152

3.2 Determination of Membrane-Associated Peptide Secondary Structure

Chemical shift measurements are widely used to obtain information on membrane-associated peptide secondary structure and to gain insight into conformational changes in transmembrane proteins as the shifts of peptide carbonyls and methyl carbons can differ by up to 8 ppm in the solid-state, based on whether that site is in an α-helical, β-sheet, or extended conformation.[21–24]

For the determination of secondary structure of peptides in membranes, labeled carbons are often not shift-resolved from the large natural abundance lipid background, as the sterol labels were above. Thus, unambiguous assignments require spectral filtering. REDOR is often used to select the peptide ^{13}C signal of interest through the strong one-bond $^{13}C-^{15}N$ dipolar coupling between the carbonyl carbon of residue i and the amide nitrogen of residue $i+1$. Weaker couplings between more distant ^{15}N and side chain ^{13}C sites can also be exploited by increasing the dipolar evolution time. Spectral editing by REDOR for chemical shift determination is demonstrated in Figure 3 for the synthetic analogue of a magainin-like antimicrobial peptide K3 known to form pores in bacterial cell membranes.

An alternative strategy for the determination of peptide conformation is based on distance measurements between selectively labeled residues.[22,25–27] A good example is the investigation of phospholamban (PLB), the 52-amino acid membrane-spanning protein with a primary role of regulating the active transport of calcium ions into the sarcoplasmic reticulum lumen via an inhibitory association with the Ca^{2+}-ATPase SERCA. In a joint rotational resonance and REDOR NMR investigation of PLB,[28] site-specific ^{13}C and ^{15}N labels were placed in the peptide backbone and the sample was reconstituted in multilamellar phospholipid vesicles in the presence and absence of SERCA. Distance measurements between [2-^{13}C]-Ala_{24} and [^{15}N]Gln_{26} by REDOR experiments revealed that unlike the $Leu_{42}-Leu_{44}$ transmembrane and the $Pro_{21}-Ala_{24}$ cytoplasmic segment of the protein, the sequence $Ala_{24}-Gln_{26}$ switches from an α-helix in pure lipid membranes to a more extended structure in the presence of the Ca^{2+}-ATPase. The results suggested local structural distortions in the polypeptide chain induced by SERCA which change the relative orientation of the transmembrane and cytoplasmic domains of PLB and may promote the association of PLB with the Ca^{2+}-ATPase.[28]

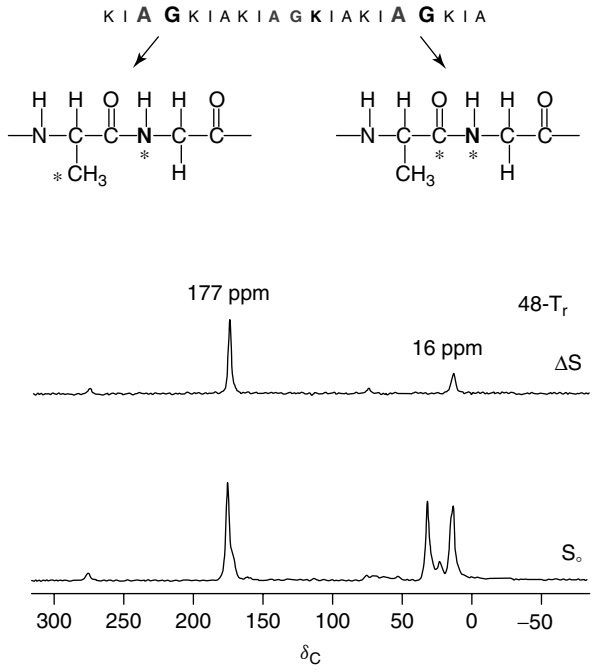

Figure 3 REDOR selection for secondary structure determination. 50-MHz $^{13}C\{^{15}N\}$ REDOR spectra of [3-^{13}C]Ala_3-[^{15}N]Gly_4-[1-^{13}C]Ala_{10}-[2-^{13}C]Gly_{11}-[6-^{15}N]Lys_{12}-[1-^{13}C]Ala_{17}-[^{15}N]Gly_{18}-K3-NH_2 incorporated into MLVs of DPPC and DPPG (1 : 1) at a lipid-to-peptide molar ratio of 10, after 48 rotor cycles of dipolar evolution with MAS at 5000 Hz. Peptide signals arising from [3-^{13}C]Ala_3 and [1-^{13}C]Ala_{17} were selected by their dipolar couplings to proximate ^{15}N spins ([^{15}N]Gly_4 and [^{15}N]Gly_{18}, respectively). Resonance lines in the ΔS spectrum at 16 and 177 ppm report an α-helical conformation for the beginning (Ala_3) and the end (Ala_{17}) of the peptide chain. The assignment of the [1-^{13}C]Ala_{17} carbon was confirmed by a 8-$T_r^{13}C$ ^{15}N REDOR experiment

3.3 Association of Polypeptide Chains in Lipid Bilayers

In addition to providing direct structural evidence for the conformation of polypeptide chains, homo- and heteronuclear dipolar recoupling experiments have proven to be powerful approaches in the determination of *intermolecular* distance restraints for peptide chains situated in membrane bilayers. These experiments have provided structural and mechanistic insights into the assembly and function of a wide range of biological systems including pore-forming antimicrobial peptides, viral coat proteins, fusion peptides, and integral membrane proteins.

In one recent investigation of PLB, Smith and coworkers used REDOR to address the structure of the pentameric complex of PLB in the region of $Gln_{22}-Gln_{29}$.[29] Three different samples were made in which specifically ^{13}C and ^{15}N glutamine-labeled PLB were reconstituted in lipid bilayers in a 1 : 1 molar ratio. The strongest dipolar coupling was measured for Gln_{29}, with an internuclear [5-^{13}C]Gln-[5-^{15}N]Gln distance of 4.1 Å ± 0.2 Å. Weaker but still observable couplings (<6 Å) were detected for Gln_{26} and Gln_{22}, altogether consistent with a hydrogen-bonded network within the central pore of the pentamer.[29]

In a similar study directed at the structural investigation of the M2 proton channel essential for influenza infection, site specific ^{15}N and ^{13}C labels were introduced at residues His_{37} and Trp_{41} into the 25-residue transmembrane segment of M2 known to form a tetrameric helical bundle. An upper limit of 3.9 Å for the interhelical [$^{15}N_\pi$]His_{37}-[$^{13}C_\gamma$]Trp_{41} distance, inferred from $^{13}C\{^{15}N\}$ REDOR experiments[30] in conjunction with the tilt and rotational angles of the helices known from previous studies,[31] was used to identify specific side-chain pairings and to characterize side-chain torsional angles for the tetrameric bundle.

In the case of PLB and M2, the ^{13}C labels were incorporated into unique amino acid side chains and were chemical-shift resolved. The strategic incorporation of labels and the application of two subsequent dipolar recoupling experiments provided an elegant way to measure intermolecular distances in the K3 antimicrobial peptide system, where ^{13}C labels

eMagRes, Online © 2007 John Wiley & Sons, Ltd.

This article was previously published in the *Encyclopedia of Magnetic Resonance* in 2010 by John Wiley & Sons, Ltd.
DOI: 10.1002/9780470034590.emrstm1152

overlapped with lipid natural abundance contributions, as illustrated in Figure 4.[32] In many of the K3 experiments, a mixture of two differently labeled peptide chains was used, with one containing a site-specific ^{19}F label. The full-echo ^{13}C spectrum (S_0) of an equimolar mixture of [1-^{13}C]Ala$_{10}$-[^{15}N]Gly$_{11}$-K3 and [3-^{19}F]Ala$_{10}$-K3 (Figure 4a) in multilamellar vesicles of DPPC and dipalmitoylphosphatidylglycerol (DPPG) is shown in the bottom of Figure 4(b). The ^{13}C carbonyl of Ala$_{10}$ was selected by the strong one-bond ^{13}C–^{15}N dipolar coupling via a short, 4-rotor cycle TEDOR coherence transfer.[14] The TEDOR coherence transfer was followed by 48 additional rotor cycles first in the absence (TEDOR-S_0, middle) then in the presence of ^{19}F dephasing pulses. The appearance of the sizable ^{15}N $\rightarrow$^{13}C{^{19}F} TEDOR-REDOR difference signal (ΔS, top) is a manifestation of the intermolecular [1-^{13}C]Ala$_{10}$-[3-^{19}F]Ala$_{10}$ dipolar coupling and unambiguously proves the proximity of the peptide chains in the bilayer. The least-square analysis of the ^{13}C{^{19}F} REDOR curve with normalized $\Delta S/S_0$ dephasing as a function of dipolar evolution time (Figure 4c) showed a bimodal distribution of [1-^{13}C]Ala$_{10}$-[3-^{19}F]Ala$_{10}$ distances: a narrow distribution centered at 4.5 Å and a broad distribution centered at 9.6 Å. The narrow distribution at short interchain distances suggested specific interactions between K3 chains whereas the broad distribution at longer distances reflected less specific association of peptide chains. As differences in sideband dephasing rates in REDOR experiments are indications of a preferred relative orientation between the chemical shift anisotropy (CSA) and dipolar tensors,[33] low-spinning experiments were used to obtain orientation restraints between K3 chains (Figure 4 d–f). In conjunction with additional measurements,[24,32] a number of distances and orientation parameters of interacting helices were used to generate a toroidal pore model for K3 that was consistent with a model originally proposed by Huang and coworkers[33] and provided further insight into the mode of action of K3 peptides.

Protegrin-1 (PG-1) is another antimicrobial peptide which, unlike K3, assumes a β-hairpin structure in lipid bilayers. In this case, REDOR was used to differentiate between the

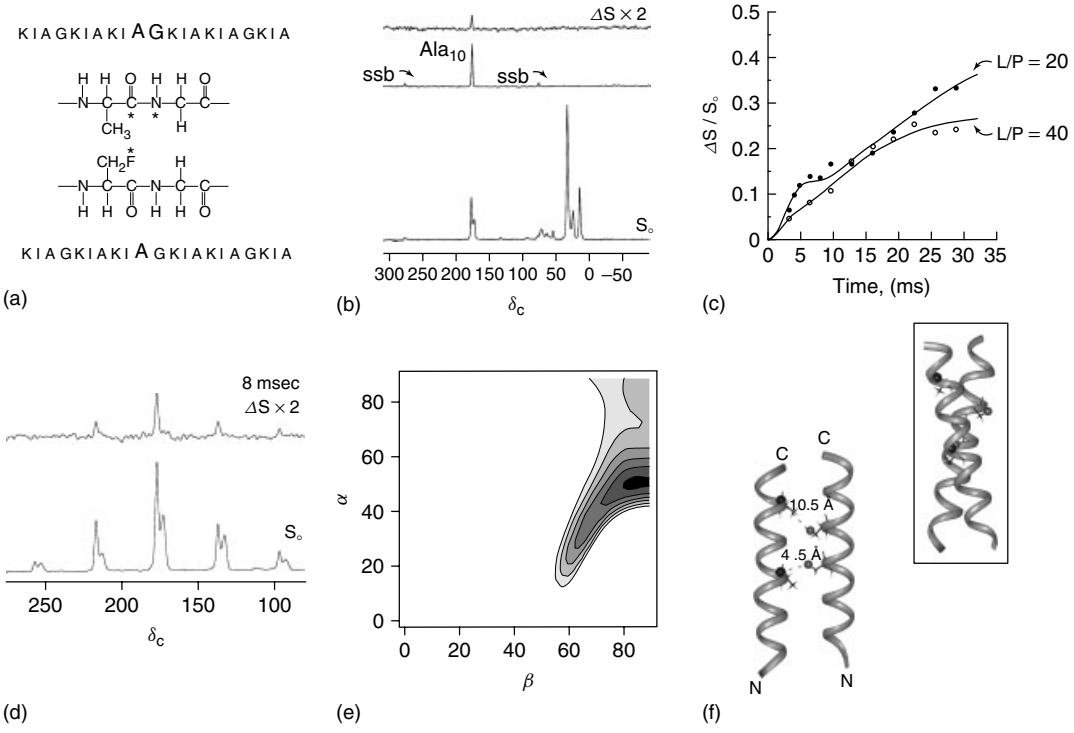

Figure 4 Aggregation study of antimicrobial peptides by REDOR. (a) Positions of the ^{13}C, ^{15}N, and ^{19}F labels in the two K3 peptide analogs used in the REDOR experiments to probe the aggregation of peptide chains. (b) 50-MHz ^{15}N $\rightarrow$^{13}C{^{19}F} TEDOR-REDOR NMR spectra of a 1 : 1 mixture of [1-^{13}C]Ala$_{10}$-[^{15}N]Gly$_{11}$-K3-NH$_2$ and [2-^{2}H, 3-^{19}F]Ala$_{10}$-K3-NH$_2$ incorporated into MLVs of DPPG/DPPC (1 : 1) at a lipid-to-peptide molar ratio (L/P) of 20 after 48 rotor cycles of dipolar evolution with MAS at 5000 Hz. The 48-T$_r$ full echo spectrum (S_0) is shown at the bottom of the figure. The middle spectrum resulted from a 4-T$_r$ ^{15}N $\rightarrow$^{13}C TEDOR coherence transfer followed by 48 additional rotor cycles with high power proton decoupling. The 48-T$_r$ REDOR ΔS spectrum of the TEDOR-selected signal is shown at the top. The deuterium label was not used in these experiments. (c) ^{13}C{^{19}F} REDOR dephasing of the 1 : 1 mixture of the two differently labeled K3 peptides embedded in MLVs of DPPG : DPPC (1 : 1) at L/P = 20 and 40. The solid lines show the calculated dephasing assuming two distributions of ^{13}C–^{19}F pair distances: one with a mean internuclear ^{13}C–^{19}F separation of 4.5 Å (width 0.7 Å), and the other with a mean of 9.6 Å (width 3.0 Å). At L/P = 20, the two distributions are about equally populated. At L/P = 40, the population with the smaller mean and narrower distribution width decreases. (d) ^{13}C{^{19}F} REDOR spectra of the K3-membrane sample at L/P = 20 after 8 ms of dipolar evolution with MAS at 2000 Hz. (e) Contour plots of the minimum root mean-square deviation error values obtained from the analysis of the sideband dephasing rates observed in ^{13}C{^{19}F} REDOR spectra of the K3-membrane complex with MAS at 2 kHz. Spectra were collected at dipolar evolution times of 4 and 8 ms. α and β are the azimuthal and polar angles, respectively, that define the orientation of the ^{13}C–^{19}F dipolar vector in the principal axis system of the ^{13}C carbonyl CSA tensor of the peptide. Each contour plot represents a 50% increase in error, with the darkest region representing the best fit. (f) Model of the dimerized K3 chains obtained from the combination of distance and angular information. The helices intersect at an approximate cross-angle of 20° (inset)

eMagRes, Online © 2007 John Wiley & Sons, Ltd.

This article was previously published in the *Encyclopedia of Magnetic Resonance* in 2010 by John Wiley & Sons, Ltd.
DOI: 10.1002/9780470034590.emrstm1152

possible packing and alignment motifs between membrane-embedded dimerized PG-1 chains.[34] Intermolecular $^{13}C-^{19}F$ and $^{15}N-^{13}C$ distance measurements were complemented by ^{15}N-detected $^{1}H\{^{13}C\}$ REDOR experiments, a modification of the original REDOR pulse sequence[17] directed at the determination of the internuclear distance between a ^{13}C label and an amide proton bonded to a ^{15}N-labeled amide. The intermolecular distances inferred from the various REDOR experiments indicated a parallel arrangement of the two protegrin-1 chains with the C-terminal strand of the hairpin forming the dimer interface. As shown by molecular modeling, the in-register arrangement of the peptide chains enhances the amphipathic character of the dimer and may facilitate its insertion into the membrane.

Using similar strategies discussed earlier for short 20–30-residue peptides, dipolar recoupling experiments have also been successfully applied to study the mechanisms of transmembrane signaling in large membrane proteins. One example is the investigation of a ligand-induced conformational change in the 60-kDa serine bacterial chemoreceptor.[35] Two mutant proteins were engineered with unique cysteine residues to permit the determination of accurate intra- and interhelical distances in the presence and absence of serine. The proteins were biosynthetically labeled with [1-^{13}C]Cys and [ring-4-^{19}F]Phe at the unique cysteine and the 13 phenylalanine positions in the protein, respectively. $^{13}C\{^{19}F\}$ REDOR measurements demonstrated that there was a 1-Å difference for the interhelical [1-^{13}C]Cys_{56}-[ring-4-^{19}F]Phe_{163} distance between the ligated and the unligated state. On the basis of the known X-ray structure of the homologous aspartate receptor, the detected 1 Å ligand-induced [1-^{13}C]Cys_{56}-[ring-4-^{19}F]Phe_{163} distance change corresponded to a 2.4-Å translation of helix 4 consistent with a previously proposed piston model[36] for the signaling mechanism. This example underscores the ability of REDOR to measure distances accurately and provides crucial information about biological function associated with distance changes that are as small as 1 Å in a 60-kDa membrane protein.

4 INSOLUBLE PEPTIDE AGGREGATES AND PEPTIDE-LATTICE INTERACTIONS

4.1 Amyloid Peptides

In the past decade, solid-state NMR has proven to be a powerful experimental approach for obtaining high-resolution structural information on the organization of insoluble fibrils produced by amyloid-forming peptides including the β-amyloid (Aβ) peptide associated with Alzheimer's disease. Multiple-quantum and REDOR measurements have shown that different amyloidogenic peptides derived from the 42-residue Aβ peptide can assemble to form fibrils containing either parallel or antiparallel β-sheets, depending on preparation conditions. This work has been pioneered in Robert Tycko's laboratory. Tycko's recent 2009 study demonstrated that Aβ fibrils seeded from human brain-extracted amyloid fibrils display structural differences compared to fibrils seeded from synthetic fibrils.[37]

While many peptides form fibril structures that tend to maximize contacts among hydrophobic residues, alternate stabilizing interactions have been proposed in peptides with low hydrophobicity such as in amyloid fibrils formed by the 20-residue segment of the asparagine- and glutamine-rich segment of the yeast prion protein Ure2p.[38] A modified REDOR scheme called "*double single-quantum*" (DSQ)-REDOR[38] was employed to reveal H-bonding between glutamine side chains in adjacent parallel β-strands in Ure2p. The observations were consistent with the "polar zipper" model of stabilizing side chain H-bonding interactions in amyloid fibrils originally proposed by Perutz.[39]

4.2 Silk Peptides

Silk fibers produced by spiders and silkworms exhibit a unique and balanced combination of strength, stiffness, and elasticity. An improved understanding of their structure-property relationships is sought to aid the molecular design of fibers with these characteristics. REDOR and other solid-state NMR techniques have provided structural constraints on model peptides for noncrystalline natural silks. Most of these studies have focused on the determination of torsional angles[40,41] and mapping of intramolecular H-bonds[42,43] by distance measurements between specifically ^{13}C and ^{15}N-labeled residues. In one application by Gullion and coworkers,[44] $^{13}C\{^{2}H\}$ REDOR was employed to investigate selectively ^{13}C, ^{2}H-labeled $(AlaGly)_{15}$ samples that serve as conformational mimics of silk I fibers. The silk I conformation has remained elusive and precedes the transition to the final β-sheet rich silk II conformation in silk fibroins from *Bombyx mori* silkworms. The REDOR data provided distances and the dihedral angles Φ and Ψ indicated the presence of a type II peptide turn in the region Gly(14)-Gly(17), which is consistent with a repeated β-turn conformation for silk I. In addition, carbon chemical shifts of the alanine residues of the silk mimic were similar to those of the natural silk I material from *Bombyx mori* silkworms and supported further the relevance of the structural parameters determined in the labeled silk mimics.

4.3 Biomineralized Peptides

Biomineralization in hard tissue is controlled by extracellular matrix proteins, which exert their action by either triggering cell signaling pathways or directly promoting or inhibiting the growth of minerals. Solid-state NMR is particularly well suited for the study of protein-surface interactions and can provide molecular-level insights into the recognition of biomineral surfaces. Statherin, a 43-amino acid salivary protein has a dual function of inhibiting both nucleation and crystal growth of hydroxyapatite (HAP), $Ca_{10}(PO_4)_6(OH)_2$, the main component of bone and teeth, via a direct interaction with the HAP surface. In a series of investigations by Drobny and coworkers,[45,46] dipolar recoupling techniques in conjunction with NMR relaxation experiments were used to characterize the conformation and dynamics of HAP-bound statherin and its N-terminal 15-residue segment, SN-15. In addition, to probe the side-chain interactions of SN-15 with HAP, internuclear distances were measured from ^{15}N in the side chain of Lys_6[47] as well as from ^{13}C spins in the side chains of Phe_7 and Phe_{14}[48] to ^{31}P spins on the HAP surface. The distance restraints obtained from REDOR experiments were used to construct a model of the surface-bound peptide, including its orientation with respect to the crystal surface.

eMagRes, Online © 2007 John Wiley & Sons, Ltd.

This article was previously published in the *Encyclopedia of Magnetic Resonance* in 2010 by John Wiley & Sons, Ltd.
DOI: 10.1002/9780470034590.emrstm1152

4.4 Biomineralized Calcite

Emiliania huxleyi is a unicellular alga (phytoplankton), prevalent in oceans, that surrounds itself with remarkable calcium carbonate structures called *coccoliths*. Schmidt and coworkers recently applied $^{13}C\{^{15}N\}$ and $^{13}C\{^{31}P\}$ REDOR to examine the composition of the coccolith calcite-rich matrix and the nature of the bioorganic–inorganic interface.[49] Isotope labels were biosynthetically incorporated by *E. huxleyi* in a medium that included, among other components, sea water, ^{15}N-enriched $Na^{15}NO_3$, and ^{13}C-enriched $NaH^{13}CO_3$. Cross polarization magic angle spinning (CPMAS) and REDOR experiments were performed to investigate both bulk crystalline and interfacial carbonate environments. REDOR measurements of intact coccoliths indicated that interfacial carbonates were not proximate to nitrogen or phosphorus atoms, within the short range of 4 Å. As part of the "full accounting" possible with REDOR in such heterogeneous biological samples, the $^{13}C\{^{15}N\}$ REDOR spectra confirmed the peptide backbone chemical-shift assignment of the sample due to one-bond dephasing of the carbonyl carbon by nitrogen, and emphasized the high degree of ^{15}N label incorporation. Using a modified REDOR protocol with direct ^{13}C excitation (rather than CP excitation), the authors observed dephasing by both ^{15}N and ^{31}P, consistent with the incorporation of small nonprotonated moieties such as PO_4^{3-} and NO_3^- as structural defects adjacent to crystalline calcite carbonates.[49]

5 PROTEIN–LIGAND INTERACTIONS

REDOR has proven to be a powerful tool for the investigation of the active sites of enzymes, in particular for the identification of the specific residues and atoms involved in ligand binding, for the measurement of specific protein-ligand distance restraints, and for probing the conformation of the enzyme-bound ligands.

5.1 Protein–Ligand Distance Restraints

The unusual eight-carbon sugar 3-deoxy-D-*manno*-2-octulosonate (KDO) is a site-specific constituent found only in Gram-negative bacteria required for lipid A maturation and cellular growth. Inhibition of its production is an attractive therapeutic strategy in the fight against Gram-negative organisms. This led to the extensive study of the mechanism of action of 3-deoxy-D-*manno*-2-octulosonate-8-phosphate synthase (KDO8PS), the enzyme responsible for the biosynthetic formation of KDO.[50–52] In a solid-state NMR investigation by Schmidt and coworkers,[53] the combination of $^{15}N\{^{31}P\}$, $^{15}N\{^{13}C\}$, $^{13}C\{^{31}P\}$ REDOR experiments were applied to the binary complexes of KDO8PS with its natural substrates, phosphoenolpyruvate (PEP) and arabinose-5-phosphate (A5P). The strategy included the preparation of uniformly ^{15}N-labeled and $[\eta\text{-}^{15}N_2]$Arg-labeled enzymes and monitoring the ^{15}N enzyme nuclei as a function of their dipolar interactions with proximate ligand ^{31}P and ^{13}C nuclei. In parallel, ^{31}P and ^{13}C NMR experiments were conducted that directly monitored the state of the ligands themselves and their proximity to the enzyme ^{15}N nuclei. The REDOR experiments have established that PEP and A5P are bound by KDO8PS via two distinct sets of Lys and Arg residues corresponding to adjacent subsites in the enzyme.[53] The solid-state NMR data complemented the crystallographic structure of KD08PS and in combination with mutagenesis results allowed the identification of specific active site residues. In the same study, a mechanism-based inhibitor of KD08PS was investigated and found to exert its action by mimicking the binding of A5P. Subsequently, the application of frequency-selective REDOR experiments provided a detailed mechanistic characterization of the inhibitor action.[11]

A similar multinuclear REDOR NMR approach was used to characterize the ternary complex of the 46-kDa enzyme 5-enolpyruvylshikimate-3-phosphate (EPSP) synthase with shikimate-3-phosphate (S3P) and *N*-(phosphonomethyl)-glycine (glyphosate or Glp).[54,55] EPSP is a key intermediate in the synthesis of aromatic amino acids in plants. Glyphosate is the active ingredient in the commercially available inhibitor of EPSP synthase, Roundup®. It binds to EPSP synthase in the presence of S3P, and inhibits the condensation of S3P and PEP to form EPSP. In REDOR investigations, designed to obtain high-resolution atomic-level structural detail of the ternary complex, interligand and ligand-protein distances were obtained from an elegant combination of labeling strategies. Multiple REDOR samples were prepared using a combination of native ^{31}P in S3P and Glp; biosynthetically ^{13}C-labeled S3P; specifically ^{13}C and ^{15}N-labeled Glp; and a variety of ^{15}N and ^{19}F-labeled EPSP synthase preparations.[56,57] Molecular modeling used multiple distance restraints measured and established the capacity of REDOR to be used in the construction of highly detailed ligand-bound molecular models in protein systems beginning with the crystal coordinates of the unliganded protein.[55]

Lumazine synthase is another key enzyme in plants and microorganisms. It is required for riboflavin synthesis and has been established as a target for antibiotic development. Unlike humans and other animals, plants and microorganisms biosynthesize vitamins and inhibition of any of the enzymes involved in the biosynthetic pathway (e.g. lumazine synthase) could result in selective toxicity to the pathogen. Thus, Schaefer, Cushman, and colleagues examined a series of metabolically stable phosphonate-reaction intermediate analogs complexed to *Saccharomyces cerevisiase* lumazine synthase in order to gain insight into key steps in catalysis which were incompletely understood. Distances from the fluorine and phosphorus atoms of the ligands to specific side chain nitrogens determined from $^{15}N\{^{19}F\}$ and $^{15}N\{^{31}P\}$ REDOR experiments were used in combination with the X-ray crystal coordinates of one of the complexes in molecular dynamics simulations to gain insight into the enzyme mechanism.[58,59]

5.2 Conformation of Bound Ligands

In the applications discussed above, REDOR was used to identify residues involved in ligand binding and to infer specific intermolecular distance restraints between the enzyme and its substrate. An equally important question in understanding enzyme mechanisms and, in a broader sense, protein–ligand interactions, is the determination of bound ligand conformations. In systems inaccessible to X-ray crystallography and solution NMR techniques, solid-state NMR experiments, and dipolar recoupling techniques

eMagRes, Online © 2007 John Wiley & Sons, Ltd.

This article was previously published in the *Encyclopedia of Magnetic Resonance* in 2010 by John Wiley & Sons, Ltd.
DOI: 10.1002/9780470034590.emrstm1152

in particular, provide a powerful alternative. For example, the determination of the structure of the microtubule-bound anticancer drug paclitaxel is of tremendous importance in order to understand its structure-based ability to bind to tubulin and to guide the development of improved and perhaps greatly simplified analogs. Paclitaxel has a relatively rigid tetracyclic ring system, but has four flexible side chains. The presence of these freely rotatable units gives rise to numerous possible conformations. Although the $\alpha\beta$-tubulin dimer structure has been solved by 2-D electron crystallography, the 3.7-Å resolution was too low to permit direct determination of the paclitaxel conformation. Two comprehensive REDOR investigations have determined the conformation of paclitaxel bound to intact microtubules. The earlier study employed a Double REDOR measurement. A single ^{19}F label was incorporated into the benzoyl moiety of paclitaxel, and specific ^{13}C and ^{15}N labels were introduced into its side chain.[15] The ^{15}N label was used for the selection of the two labeled ^{13}C sites via their one-bond ^{13}C-^{15}N dipolar couplings, allowing the assignment of the peaks in the ^{13}C{^{19}F} REDOR difference spectrum and determination of the couplings and distances. Thus, two distance restraints were obtained for two shift-resolved carbons in the taxol molecule by ^{15}N selection amidst the megadalton natural abundance ^{13}C background of microtubules.

More recently, the use of TEDOR-REDOR has been employed to achieve this type of selection rather than Double REDOR, and is highlighted in sections "Membrane Peptides, Proteins, and Sterols" and "Bacterial Metabolism, Cell Walls, and Antibiotics". In conjunction with fluorescence spectroscopic data and molecular modeling, the determined ^{13}C–^{19}F intramolecular distance restraints allowed the refinement of the microtubule-bound conformation of paclitaxel and suggested a T-shaped model for the orientation of the ligand in the binding site. In the more recent study, experimental results from ^{2}H{^{19}F} REDOR NMR provided direct confirmation that paclitaxel adopts a T-shaped conformation when it is bound to tubulin.[61] ^{2}H{^{19}F} REDOR is an attractive measurement as there are no natural abundance contributions in the sample. As a remarkable demonstration of a structure-based medicinal chemistry approach and the importance of the results generated with REDOR, a potent and structurally constrained paclitaxel analog based on the REDOR model was synthesized by Ojima and coworkers.[62,63]

Double REDOR experiments (^{13}C{^{15}N} followed by ^{13}C{^{19}F}) were also carried out in combination with molecular dynamics simulations to gain insight into the conformation of bound amidine and amidine-imidazoline inhibitors of human Factor Xa, a 45-kDa enzyme acting at the early stages in the blood-coagulation cascade.[64,65] Yet another example is the REDOR-based model of noncovalent H^+/K^+-ATPase inhibitor analogues established by Watts and coworkers.[66] In this study, dipolar couplings between ^{19}F in the benzyl ring and ^{13}C placed in the N–CH_3 group of the quaternary ammonium cation were measured to probe the relative orientations of the phenylmethoxy group and the imidazopyridine ring of the inhibitor. In combination with previous information on the torsional angle Φ_1,[67] the results of the ^{13}C{^{19}F} REDOR measurements, which probed torsional angles Φ_2 and Φ_3, were used to confine the bound inhibitor to a small cluster of structures.

6 NUCLEIC ACID INTERACTIONS

REDOR has increasingly been used in recent years to examine various interactions involving DNA and RNA. These include the investigation of drug-DNA, enzyme-nucleotide complexes, RNA-peptide structures, as well as interactions involved in viral capsid DNA packaging. In the realm of drug-DNA investigations, REDOR was used to map the binding of a fluorine-substituted quinobenzoxazine to a DNA G-quadruplex labeled by phosphothioation and [methyl-^{13}C]thymidine.[68] G-quadruplexes have emerged as a target for anticancer drug development. In this example by Schaefer-Hurley, ^{31}P{^{19}F} and ^{13}C{^{19}F} REDOR were used to measure distances from fluorine in the compound to ^{31}P and ^{13}C labels in the quadruplex. Earlier, Drobny's group also used ^{31}P{^{19}F} REDOR to examine the binding of the drug distamycin in the DNA minor groove as a function of the drug-DNA stoichiometry.[60]

Uracil is not a natural DNA base, but is introduced into the genome by spontaneous damage that is repaired by the important enzyme uracil DNA glycosylase (UDG). UDG selectively recognizes and excises the unwanted uracil bases from DNA in a process that involves damaged base pair flipping. REDOR measurements contributed to results from solution ^{19}F NMR and binding affinity measurements to probe the mechanism of uracil recognition and the pathway of base flipping by UDG.[69] The study by Schaefer, Stivers, and coworkers characterized the molecular details of how UDG achieves its specificity by the recognition of the shapes and certain types of molecular defects. ^{31}P{^{19}F} REDOR data were used to narrow down which of several structural models for the enzyme-complexed DNA were appropriate by comparing the experimental REDOR dephasing with calculated dephasing values based on the atomic coordinates of the structural models.

The Drobny laboratory investigated a complex of the HIV transactivation response element (TAR) RNA with a short peptide segment from the binding domain of the viral regulatory protein tat.[70] Although related complexes had been studied extensively by solution-state NMR, crystallography, and other biophysical techniques, peptide motion and other challenges had hindered observations of contacts between HIV-1 TAR with tat peptides. This situation made solid-state NMR a natural choice for the problem. The NMR labeling approach involved the incorporation of site-specific ^{19}F and ^{31}P nuclei into the tat binding site of the 29-residue HIV-1 TAR RNA construct. ^{31}P{^{19}F} REDOR was used to determine conformational changes accompanying peptide binding. The ^{31}P–^{19}F distance between the incorporated phosphorothioate (pS) 5′ of A27 and the 2′-fluoro-2′-deoxyuridine introduced at the bulge residue U23 changed significantly, from 10.3 Å in the unbound RNA to 6.6 Å following the binding of the tat peptide (Figure 5). The results were used to refine previous solution NMR studies that indicated a sizable rearrangement at the TAR RNA binding site upon addition of the peptide.

In a more recent study, the combination of ^{15}N{^{31}P} and ^{31}P{^{15}N} REDOR experiments were used to address various aspects of DNA packaging in bacteriophage T4.[72] Experiments were carried out uniformly on ^{15}N- and [ε-^{15}N]lysine-labeled bacteriophage T4. In addition, to determine the charge-screening effect of monovalent cations,

eMagRes, Online © 2007 John Wiley & Sons, Ltd.

This article was previously published in the *Encyclopedia of Magnetic Resonance* in 2010 by John Wiley & Sons, Ltd.
DOI: 10.1002/9780470034590.emrstm1152

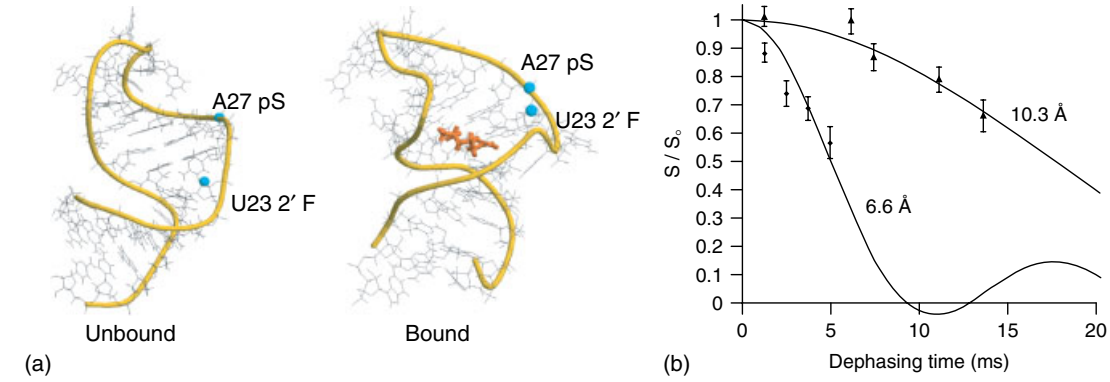

Figure 5 Peptide–RNA interactions by REDOR. (a) Conformations of TAR RNA in the unbound form (left) and when bound to the tat peptide (right) determined by solution NMR and molecular modeling.[70,71] The phosphate backbone is represented by yellow ribbons. Blue spheres denote the 2-^{19}F U23 and pSA27 label positions used in the solid-state NMR work. (b) ^{31}P{^{19}F} REDOR dephasing of TAR RNA in the absence and in the presence of 1.2 equivalents of tat peptide. Solid lines show calculated dephasing for ^{31}P–^{19}F distances of 10.3 Å and 6.6 Å between the ^{19}F-labeled U23 and the pSA27 site of TAR RNA in its free and tat-bound form. The ^{31}P–^{19}F distances determined by REDOR were in agreement with the solution NMR-derived model

$^{15}NH_4^+$ was introduced into filled, unlabeled capsids from synthetic medium by exchange. ^{15}N{^{31}P} REDOR measurements were used to determine whether the encapsulated T4 dsDNA was present in A-DNA or B-DNA conformations. Nitrogen–phosphorus distances differ for the two forms due to differences in sugar conformations,[73,74] and the ^{15}N{^{31}P} REDOR experiments proved that the encapsulated T4 dsDNA was in an unperturbed B-DNA conformation.[72] By characterizing the contacts between amines and DNA phosphates, Yu and Schaefer also demonstrated that the DNA phosphate negative charge is balanced by lysyl amines, polyamines, and monovalent cations. Neither arginine nor histidine side-chain nitrogen atoms showed significant contact with DNA phosphates, suggesting that they are not actively involved in DNA charge neutralization in T4. It was also shown that a little over 10% of lysyl amines, 40% of -NH_2 groups of polyamines, and 80% of monovalent cations within the lyophilized T4 capsid were involved in DNA charge balance. The NMR data suggest that DNA enters the T4 capsid in a charge-unbalanced state. The investigators proposed a model in which the repulsive force due to the negatively charged entry channel provides free energy to accelerate the packaging of DNA.

7 BACTERIAL METABOLISM, CELL-WALLS, AND ANTIBIOTICS

REDOR has been used extensively to investigate cell-wall architecture and whole-cell metabolism in bacteria, with an emphasis on understanding antibiotic modes of action. CPMAS techniques were used by Schaefer's group to study bacterial metabolism as early as 1982. With the introduction of REDOR in 1989, new questions regarding metabolism and structure could be addressed and answered. In the first applications of REDOR to examine bacterial cell walls (1991–1993), Schaefer and coworkers characterized cross-linking in *Bacillus subtilis*[75] and serine metabolism in *Klebsiella pneumoniae*.[76] These applications used selective isotope labeling strategies, often incorporating one or two selectively labeled amino acids, and then used REDOR for the selection of directly bonded ^{13}C–^{15}N pairs to identify and track covalent cross-link formation and routing of the isotope labels during cell-wall metabolism. Many antibiotics target biosynthesis of bacterial cell walls, and the ability to characterize cell-wall composition and structure in a non perturbative manner is often crucial in understanding drug modes of action and developing new generation therapeutics. Schaefer and coworkers have contributed a comprehensive series of studies using REDOR to investigate cell-wall assembly in *Staphylococcus aureus* and *Enterococcus faecalis* and to dissect the modes of action of vancomycin and potent vancomycin analogues, e.g., oritavancin, that are under development for the treatment of life-threatening vancomycin-resistant staphylococcal and enterococcal infections.[77–84] In one study, REDOR was used to profile mature cell-wall components and cell-wall precursors and demonstrated that oritavancin treatment results in interference with transglycosylation and transpeptidation during cell-wall assembly in *S. aureus*.[81] To understand the molecular nature of the mode of action of oritavancin, a molecular model of the potent vancomycin analogue bound to *S. aureus* peptidoglycan was generated from a combination of measurements in intact cell walls and whole cells.[78,79,85] Among these was the first TEDOR-REDOR measurement in whole cells (Figure 6) which generated a crucial distance of 7.4 Å from the drug ^{19}F to a unique type of nucleus in the whole-cell (the crosslinked D-[1-^{13}C]Ala carbonyl carbon).[78] The collective data and resulting molecular model revealed a secondary binding site in the peptidoglycan which could only be observed in unperturbed cell walls that retained their 3-D architecture, complete with cross-linked peptide stems and compact pentaglycine bridges, which are not maintained in cell-wall mimics used for solution-based measurements.

8 PLANT METABOLISM

Schaefer and coworkers made contributions to plant biology through the 1970s and 1980s using CPMAS and techniques such as double cross polarization. More recently, in 2005–2006, Cegelski and Schaefer provided detailed information regarding glycine metabolism in growing soybean

DOI: 10.1002/9780470034590.emrstm1152

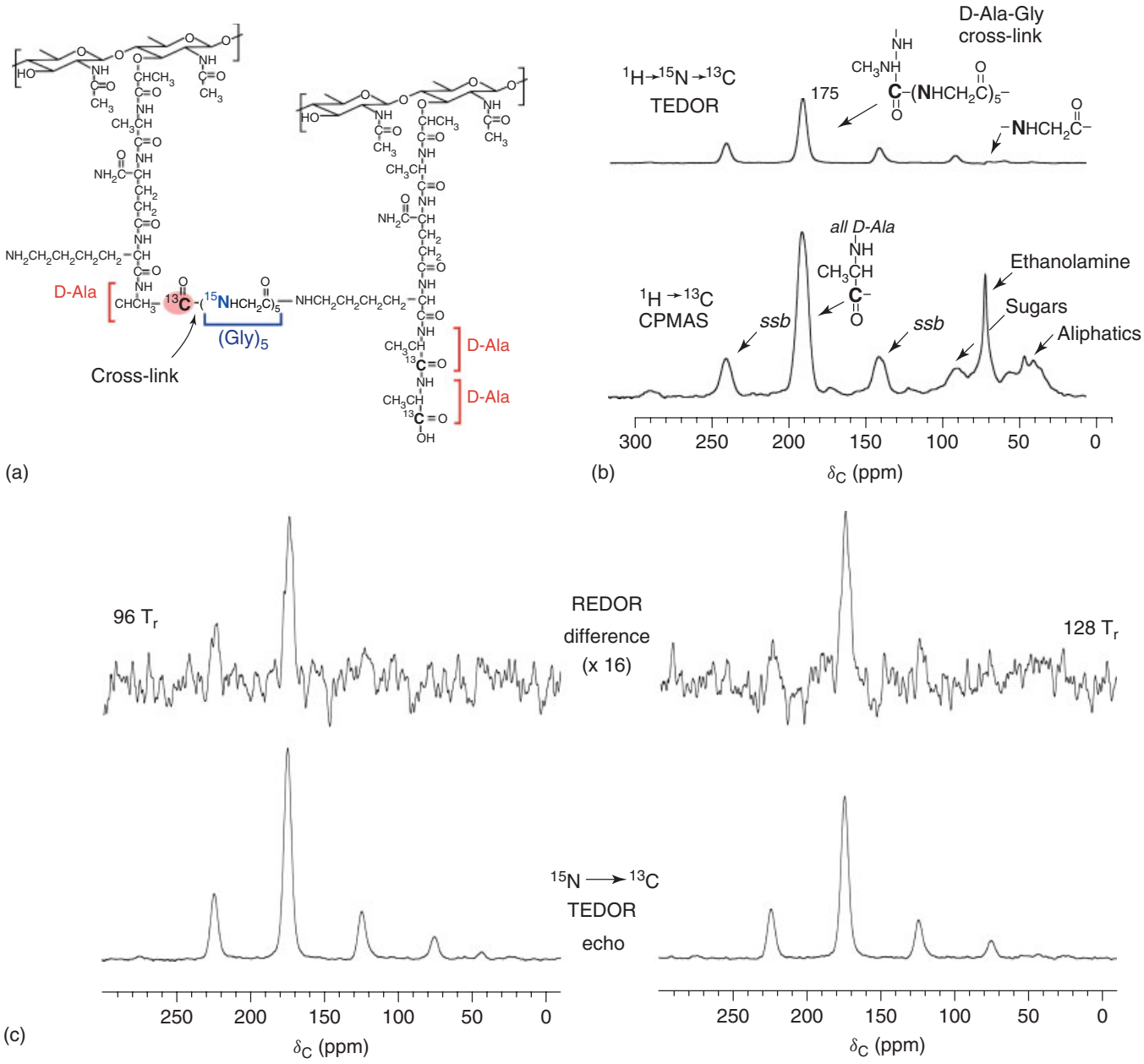

Figure 6 Whole-cell TEDOR-REDOR. (a) Peptidoglycan schematic highlighting D–[1-^{13}C]Ala and [^{15}N]Gly labels incorporated biosynthetically during growth in *S. aureus*. (b) 125-MHz CPMAS ^{13}C NMR spectrum of lyophilized sample of [^{19}F]oritavancin complexed with S. *aureus* whole cells grown on media containing D-[1-^{13}C]Ala, [^{15}N]Gly, and an alanine racemase inhibitor. The spectrum resulted from the accumulation of 256 scans. (Top) TEDOR ^{13}C NMR spectrum of the same whole-cell sample. The observed signals arise only from label and natural-abundance ^{13}C that is covalently bonded to ^{15}N. The spectrum resulted from the accumulation of 120,000 scans. (c) ^{15}N $\rightarrow$ ^{13}C{^{19}F} TEDOR-selected REDOR spectra of the whole-cell sample of Figure 6(b) after dipolar evolution for (left) 96 rotor cycles and (right) 128 rotor cycles. TEDOR full echoes (S_0) are shown at the bottom of the figure and the REDOR differences at the top of the figure. Each spectrum resulted from the accumulation of 120,000 scans. MAS was at 6250 Hz. (d) ^{15}N $\rightarrow$ ^{13}C{^{19}F} TEDOR-selected REDOR integrated dephasing ($\Delta S/S_0$) of the whole-cell sample of Figure 6(b) as a function of dipolar evolution time. The estimated error is within the size of the solid symbols. The calculated dephasing for a 7-Å single distance from the fluorine of [^{19}F]oritavancin to the ^{13}C-labeled carbonyl carbon of the cross-link site (dashed line) does not match the experimental dephasing as well as that calculated using a Gaussian distribution of distances centered at 7.4 Å (inset). The dotted lines show the calculated dephasing for single distances of 6.5 Å (upper) and 7.5 Å (lower). (e) Molecular model of the binding of [^{19}F]oritavancin in the mature cell walls of *S. aureus* generated from several distance measurements including the featured TEDOR-REDOR 7.4 Å distance

eMagRes, Online © 2007 John Wiley & Sons, Ltd.

This article was previously published in the *Encyclopedia of Magnetic Resonance* in 2010 by John Wiley & Sons, Ltd.
DOI: 10.1002/9780470034590.emrstm1152

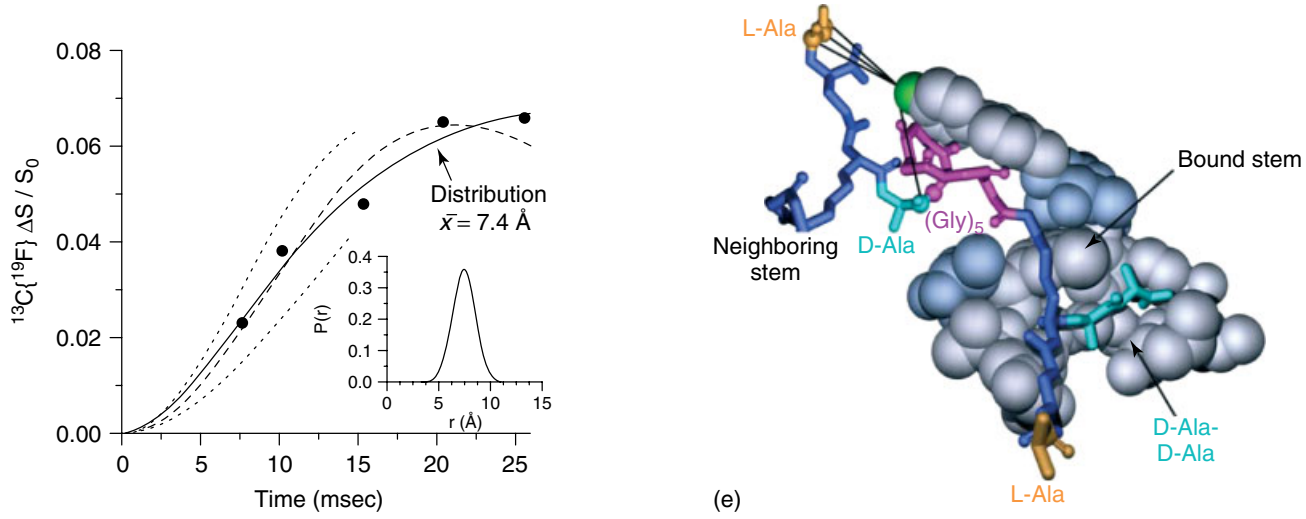

Figure 6 *continued*

plants as a function of CO_2 concentration.[12] They correlated carbon and nitrogen metabolism to track the fate of excess glycine in the leaf after short labeling times with $^{13}CO_2$ in soybean plants that were fertilized and labeled with ^{15}N-labeled ammonium nitrate. They used Dante-based frequency-selective $^{13}C\{^{15}N\}$ REDOR to identify and distinguish free glycine levels from glycine that had been incorporated into protein as a function of CO_2 concentration, in the intact-leaf spectra. At subambient CO_2 concentrations, which typically occur as the result of water stress, a significant fraction of excess glycine produced during photorespiration was incorporated into leaf protein with a high glycine, high α-helix content, typical of cell-wall proteins.[12] This work suggested that photorespiration may be of value to plants, consistent with the persistence of the pathway after a billion years of evolution.

REDOR was also employed to make a quantitative determination of the extent of photorespiration in soybean plants.[86] The measurements of intact soybean leaves labeled by $^{13}CO_2$ lead to the conclusion that photorespiration was 17% of photosynthesis and was made by two independent NMR methods. In the first, ^{13}C $\{^{31}P\}$ REDOR provided the full analysis by tracking the incorporation of ^{13}C label into sugar intermediates in the Calvin cycle as a function of time. For labeling times of five minutes or less, the isotopic enrichment of the Calvin cycle depends on the flux of labeled carbon from $^{13}CO_2$, relative to the flux of unlabeled carbon from glycerate returned from the photorespiratory cycle. Comparisons of these two rates for a fixed value of the $^{13}CO_2$ concentration indicated that the ratio of the rate of photosynthesis to the rate of photorespiration of ribulose-1,5-bisphosphate carboxylase/oxygenase (Rubisco) in soybean leaves was 6 : 1 under ambient conditions. In the second NMR method, the apparent carbon assimilation was determined from a total ^{13}C-label spin count. The ^{13}C measurement was converted to the net carbon ($^{12}C+^{13}C$) assimilation using the isotopic enrichment of the Calvin cycle known from the REDOR measurement. This method provided a complete accounting of all the ^{13}C label in the leaf and yielded the identical conclusion that the ratio of photosynthesis to photorespiration in soybean leaves was 6 : 1 under normal atmospheric conditions.[86] Again, as in most REDOR investigations, the labeling strategy and selection of the particular REDOR measurement were crucial to the overall problem-solving efforts.

9 RELATED ARTICLES

Magic Angle Spinning; Membrane Proteins; REDOR and TEDOR; Rotational Resonance in Biology; Solid Biopolymers; Structure Determination of Solid Proteins Using MAS and Isotopic Enrichment; Structure and Dynamics of Proteins Adsorbed at Biomaterial Interfaces; Structure of Silk Using Solid-State NMR

10 REFERENCES

1. T. Gullion and J. Schaefer, *J. Magn. Reson.*, 1989, **81**, 196–200.
2. R. D. O'Connor and J. Schaefer, *J. Magn. Reson.*, 2002, **154**, 46–52.
3. Y. Ishii, J. J. Balbach, and R. Tycko, *Chem. Phys.*, 2001, **266**, 231–236.
4. C. M. Rienstra, M. E. Hatcher, L. J. Mueller, B. Sun, S. W. Fesik, and R. G. Griffin, *J. Am. Chem. Soc*, 1998, **120**, 10602–10612.
5. T. Gullion, D. B. Baker, and M. S. Conradi, *J. Magn. Reson.*, 1990, **89**, 479–484.
6. A. K. Mehta and J. Schaefer, *J. Magn. Reson.*, 2003, **163**, 188–191.
7. S. Matsuoka, H. Ikeuchi, Y. Umegawa, N. Matsumori, and M. Murata, *Bioorg. Med. Chem.*, 2006, **14**, 6608–6614.
8. G. A. Morris and R. Freeman, *J. Magn. Reson.*, 1978, **29**, 433–462.
9. V. Bork and J. Schaefer, *J. Magn. Reson.*, 1988, **78**, 348–354.
10. R. J. Auchus, D. F. Covey, V. Bork, and J. Schaefer, *J. Biol. Chem.*, 1988, **263**, 11640–11645.
11. L. Kaustov, S. Kababya, V. Belakhov, T. Baasov, Y. Shoham, and A. Schmidt, *J. Am. Chem. Soc.*, 2003, **125**, 4662–4669.
12. L. Cegelski and J. Schaefer, *J. Biol. Chem.*, 2005, **280**, 39238–39245.
13. C. P. Jaroniec, B. A. Tounge, J. Herzfeld, and R. G. Griffin, *J. Am. Chem. Soc.*, 2001, **123**, 3507–3519.

DOI: 10.1002/9780470034590.emrstm1152

14. A. W. Hing, S. Vega, and J. Schaefer, *J. Magn. Reson.*, 1992, **96**, 205–209.
15. Y. Li, B. Poliks, L. Cegelski, M. Poliks, Z. Gryczynski, G. Piszczek, P. G. Jagtap, D. R. Studelska, D. G. I. Kingston, J. Schaefer, and S. Bane, *Biochemistry*, 2000, **39**, 281–291.
16. D. T. Graesser, B. J. Wylie, A. J. Nieuwkoop, W. T. Franks, and C. M. Rienstra, *Magn. Reson. Chem.*, 2007, **45**, S129–S134.
17. K. Schmidt-Rohr and M. Hong, *J. Am. Chem. Soc.*, 2003, **125**, 5648–5649.
18. K. Saalwachter and I. Schnell, *Solid State Nucl. Magn. Reson.*, 2002, **22**, 154–187.
19. N. Sinha and M. Hong, *Chem. Phys. Lett.*, 2003, **380**, 742–748.
20. L. Cegelski, C. V. Rice, R. D. O'acuteConnor, A. L. Caruano, G. P. Tochtrop, Z. Y. Cai, D. F. Covey, and J. Schaefer, *Drug Dev. Res.*, 2005, **66**, 93–102.
21. M. L. Bodner, C. M. Gabrys, P. D Parkanzky, J. Yang, C. A. Duskin, and D. P. Weliky, *Magn. Reson. Chem.*, 2004, **42**, 187–194.
22. F. Porcelli, B. Buck, D.-K. Lee, K.J. Hallock, A. Ramamoorthy, and G. Veglia, *J. Biol. Chem.*, 2004, **279**, 45815–45823.
23. A. James Mason and G. J. T. Clemens Glaubitz, *FEBS J.*, 2005, **272**, 2152–2164.
24. O. Toke, W. L. Maloy, S. J. Kim, J. Blazyk, and J. Schaefer, *Biophys. J.*, 2004, **87**, 662–674.
25. D. J. Hirsh, J. Hammer, W. L. Maloy, J. Blazyk, and J. Schaefer, *Biochemistry*, 1996, **35**, 12733–12741.
26. E. S. Karp, E. K. Tiburu, S. Abu-Baker, and G. A. Lorigan, *Biochim. Biophys. Acta*, 2006, **1758**, 772–780.
27. Y. Todokoro, I. Yumen, K. Fukushima, S.-W. Kang, J.-S Park, T. Kohno, K. Wakamatsu H. Akutsu, and T. Fujiwara, *Biophys. J.*, 2006, **91**, 1368–1379.
28. E. Hughes and D. A. Middleton, *J. Biol. Chem.*, 2003, **278**, 20835–20842.
29. W. Liu, J. Z. Fei, T. Kawakami, and S. O. Smith, *Biochim. Biophys. Acta*, 2007, **1768**, 2971–2978.
30. K. Nishimura, S. G. Kim, L. Zhang, and T. A. Cross, *Biochemistry*, 2002, **41**, 13170–13177.
31. J. F. Wang, S. Kim, F. Kovacs, and T. A. Cross, *Protein Sci.*, 2001, **10**, 2241–2250.
32. O. Toke, R.D. O'Connor, T. K. Weldeghiorghis, W. L. Maloy, R. W. Glaser, A. S. Ulrich, and J. Schaefer, *Biophys. J.*, 2004, **87**, 675–687.
33. H. W. Huang, *Biochemistry*, 2000, **39**, 8347–8352.
34. R. Mani, M. Tang, X. Wu, J. J. Buffy, A. J. Waring, M. A. Sherman, and M. Hong, *Biochemistry*, 2006, **45**, 8341–8349.
35. O. J. Murphy, F. A. Kovacs, E. L. Sicard, and L. K. Thompson, *Biochemistry*, 2001, **40**, 1358–1366.
36. S. A. Chervitz and J. J. Falke, *Proc. Natl. Acad. Sci. U.S.A.*, 1996, **93**, 2545–2550.
37. A. K. Paravastu, I. Qahwash, R. D. Leapman, S. C. Meredith, and R. Tycko, *Proc. Natl. Acad. Sci. U.S.A.*, 2009, **106**, 7443–7448.
38. J. C. C. Chan, N. A. Oyler, W. M. Yau, and R. Tycko, *Biochemistry*, 2005, **44**, 10669–10680.
39. M. F. Perutz, T. Johnson, M. Suzuki, and J. T. Finch, *Proc. Natl. Acad. Sci. U.S.A.*, 1994, **91**, 5355–5358.
40. J. Ashida, K. Ohgo, K. Komatsu, A. Kubota, and T. Asakura, *J. Biomol. NMR*, 2003, **25**, 91–103.
41. Y. Nakazawa and T. Asakura, *J. Am. Chem. Soc.*, 2003, **125**, 7230–7237.
42. T. Asakura, J. Ashida, T. Yamane, T. Kameda, Y. Nakazawa, K. Ohgo, and K. Komatsu, *J. Mol. Biol.*, 2001, **306**, 291–305.
43. T. Kameda, C. Zhao, J. Ashida, and T. Asakura, *J. Magn. Reson.*, 2003, **160**, 91–96.
44. T. Gullion, R. Kishore, and T. Asakura, *J. Am. Chem. Soc.*, 2003, **125**, 7510–7511.
45. W. J. Shaw, J. R. Long, A. A. Campbell, P. S. Stayton, and G. P. Drobny, *J. Am. Chem. Soc.*, 2000, **122**, 7118–7119.
46. J. R. Long, W. J. Shaw, P. S. Stayton, and G. P. Drobny, *Biochemistry*, 2001, **40**, 15451–15455.
47. J. M. Gibson, V. Raghunathan, J. M. Popham, P. S. Stayton, and G. P. Drobny, *J. Am. Chem. Soc.*, 2005, **127**, 9350–9351.
48. J. M. Gibson, J. M. Popham, V. Raghunathan, P. S. Stayton, and G. P. Drobny, *J. Am. Chem. Soc.*, 2006, **128**, 5364–5370.
49. R. Gertman, I. Ben Shir, S. Kababya, and A. Schmidt, *J. Am. Chem. Soc.*, 2008, **130**, 13425–13432.
50. G. D. Dotson, P. Nanjappan, M. D. Reily, and R. W. Woodard, *Biochemistry*, 1993, **32**, 12392–12397.
51. L. Hedstrom and R. Abeles, *Biochem. Biophys. Res. Commun.*, 1988, **157**, 816–820.
52. G. D. Dotson, R. K. Dua, J. C. Clemens, E. W. Wooten, and R. W. Woodard, *J. Biol. Chem.*, 1995, **270**, 13698–13705.
53. L. Kaustov, S. Kababya, S. Du, T. Baasov, S. Gropper, Y. Shoham, and A. Schmidt, *Biochemistry*, 2000, **39**, 14865–14876.
54. L. M. McDowell, B. Poliks, D.R. Studelska, R.D. O'Connor, D.D Beusen, and J. Schaefer, *J. Biomol. NMR*, 2004, **28**, 11–29.
55. L. M. McDowell, D. R. Studelska, B. Poliks, R. D. O'Connor, and J. Schaefer, *Biochemistry*, 2004, **43**, 6606–6611.
56. L. M. McDowell, A. Schmidt, E. R. Cohen, D. R. Studelska, and J. Schaefer, *J. Mol. Biol.*, 1996, **256**, 160–171.
57. D. R. Studelska, C. A. Klug, D. D. Beusen, L. M. McDowell, and J. Schaefer, *J. Am. Chem. Soc.*, 1996, **118**, 5476–5477.
58. A. K. Mehta, D.R Studelska, M. Fischer, A. Giessauf, K. Kemter, A. Bacher, M. Cushman, and J. Schaefer, *J. Org. Chem.*, 2002, **67**, 2087–2092.
59. T.-Y. Yu, R.D. O'Connor, A.C. Sivertsen, C. Chiauzzi, B. Poliks, M. Fischer, A. Bacher, I. Haase, M. Cushman, and J. Schaefer, *Biochemistry*, 2008, **47**, 13942–13951.
60. G. L. Olsen, E. A. Louie, G. P. Drobny, and S. T. Sigurdsson, *Nucleic Acids. Res.*, 2003, **31**, 5084–5089.
61. Y. Paik, C. Yang, B. Metaferia, S. Tang, S. Bane, R. Ravindra, N. Shanker, A. A. Alcaraz, S.A. Johnson, J. Schaefer, R. D. O'Connor, L. Cegelski, J. P. Snyder, and D. G. I. Kingston, *J. Am. Chem. Soc.*, 2007, **129**, 361–370.
62. R. Geney, L. Sun, P. Pera, R. J. Bernacki, S. Xia, S. B. Horwitz, C. L. Simmerling, and I. Ojima, *Chem. Biol.*, 2005, **12**, 339–348.
63. L. Sun, X. Geng, R. Geney, Y. Li, C. Simmerling, Z. Li, J. W. Lauher, S. Xia, S. B. Horwitz, J. M. Veith, P. Pera, R. J. Bernacki, and I. Ojima, *J. Org. Chem.*, 2008, **73**, 9584–9593.
64. L. M. McDowell, M. A. McCarrick, D. R. Studelska, R. D. O'Connor, D. R. Light, W. J. Guilford, D. Arnaiz, M. Adler, J. L. Dallas, B. Poliks, and J. Schaefer, *J. Med. Chem.*, 2003, **46**, 359–363.
65. D. R. Studelska, L. M. McDowell, M. Adler, R. D. O'Connor, A. K. Mehta, W. J. Guilford, J. L. Dallas, D. Arnaiz, D. R. Light, and J. Schaefer, *Biochemistry*, 2003, **42**, 7942–7949.
66. J. A. Watts, A. Watts, and D. A. Middleton, *J. Biol. Chem.*, 2001, **276**, 43197–43204.
67. D. A. Middleton, R. Robins, X. Feng, M. H. Levitt, I. D. Spiers, C. H. Schwalbe, D. G. Reid, A. Watts, *FEBS Lett.*, 1997, **410**, 269–274.
68. A. K. Mehta, Y. Shayo, H. Vankayalapati, L. H. Hurley, and J. Schaefer, *Biochemistry*, 2004, **43**, 11953–11958.

DOI: 10.1002/9780470034590.emrstm1152

69. Y. L. Jiang, L. M. McDowell, B. Poliks, D. R. Studelska, C. Cao, G. S. Potter, J. Schaefer, F. Song, and J. T. Stivers, *Biochemistry*, 2004, **43**, 15429–15438.
70. G. L. Olsen, T. E. Edwards, P. Deka, G. Varani, S.Th. Sigurdsson, and G. P. Drobny, *Nucleic Acids Res.*, 2005, **33**, 3447–3454.
71. A. S. Brodsky and J. R. Williamson, *J. Mol. Biol.*, 1997, **267**, 624–639.
72. T. Y. Yu and J. Schaefer, *J. Mol. Biol.*, 2008, **382**, 1031–1042.
73. J. M. Berg, J. L. Tymoczko, and L. Stryer, *Biochemistry, 1 v. (Various Pagings)*, W.H. Freeman: New York, 2007.
74. W. Saenger, *Principles of Nucleic Acid Structure*, Springer-Verlag: New York, 1984, Vol. xx, p. 556.
75. Y. Pan, N. S. Shenouda, G. E. Wilson, and J. Schaefer, *J. Biol. Chem.*, 1993, **268**, 18692–18695.
76. L. M. Mcdowell, E. R. Cohen, and J. Schaefer, *J. Biol. Chem.*, 1993, **268**, 20768–20771.
77. L. Cegelski, S. J. Kim, A. W. Hing, D. R. Studelska, R. D. O'Connor, A. K. Mehta, and J. Schaefer, *Biochemistry*, 2002, **41**, 13053–13058.
78. L. Cegelski, D. Steuber, A. K. Mehta, D. W. Kulp, P. H. Axelsen, and J. Schaefer, *J. Mol. Biol.*, 2006, **357**, 1253–1262.
79. S. J. Kim, L. Cegelski, M. Preobrazhenskaya, and J. Schaefer, *Biochemistry*, 2006, **45**, 5235–5250.
80. S. J. Kim, S. Matsuoka, G. J. Patti, and J. Schaefer, *Biochemistry*, 2008, **47**, 3822–3831.
81. S. J. Kim, L. Cegelski, D. Stueber, M. Singh, E. Dietrich, K. S. E. Tanaka, T. R. Parr Jr, A. R. Far, and J. Schaefer, *J. Mol. Biol.*, 2008, **377**, 281–293.
82. G. J. Patti, S. J. Kim, and J. Schaefer, *Biochemistry*, 2008, **47**, 8378–8385.
83. S. J. Kim and J. Schaefer, *Biochemistry*, 2008, **47**, 10155–10161.
84. S. Sharif, S. J. Kim, H. Labischinski, and J. Schaefer, *Biochemistry*, 2009, **48**, 3100–3108.
85. S. J. Kim, L. Cegelski, D. R. Studelska, R. D. O'Connor, A. K. Mehta, and J. Schaefer, *Biochemistry*, 2002, **41**, 6967–6977.
86. L. Cegelski and J. Schaefer, *J. Magn. Reson.*, 2006, **178**, 1–10.

Acknowledgments

We gratefully acknowledge Professor Jacob Schaefer for many insightful discussions. L.C. holds a Career Award at the Scientific Interface from the Burroughs Wellcome Fund. O.T. is supported by grants from the Hungarian Research Fund (OTKA) F68326 and the Hungarian GVOP-3.2.1.-2004-04-0210/3.0 project.

eMagRes, Online © 2007 John Wiley & Sons, Ltd.

This article was previously published in the *Encyclopedia of Magnetic Resonance* in 2010 by John Wiley & Sons, Ltd.
DOI: 10.1002/9780470034590.emrstm1152